Word Count: 5094 **Revision 1**

Redox control and measurement in low-temperature (< 450 °C) hydrothermal experiments

Jing Fang[a,b] and I-Ming Chou[a*]

[a] CAS Key Laboratory of Experimental Study under Deep-sea Extreme Conditions, Institute of Deep-sea Science and Engineering, Chinese Academy of Sciences, Sanya, Hainan 572000, China

[b] University of Chinese Academy of Sciences, Beijing 100871, China

[*] **Corresponding author.** Tel.: +86 18689673718; fax: +86 898-88384757.

E-mail address: imchou@idsse.ac.cn (I.M. Chou).

This is the peer-reviewed, final accepted version for American Mineralogist, published by the Mineralogical Society of America.
The published version is subject to change. Cite as Authors (Year) Title. American Mineralogist, in press.
DOI: https://doi.org/10.2138/am-2021-7687. http://www.minsocam.org/

Abstract

Redox control in hydrothermal experiments is routinely achieved through double-capsule and Shaw membrane techniques. These techniques control oxygen fugacity (f_{O_2}) by imposing a defined hydrogen fugacity (f_{H_2}) on a studied sample enclosed, together with H_2O, in a hydrogen membrane capsule made of Pt or Ag-Pd alloys. However, due to the low permeability of these membranes to H_2 at low temperatures (*T*), these techniques do not work efficiently below 450 °C. Here, we tested fused silica as a new hydrogen membrane and successfully applied it to monitor and control the redox states of studied samples at *T* down to 200 °C in hydrothermal experiments. Our results showed that 3, 8, 16, 36, 96, and 216 hours are sufficient for a fused silica capillary capsule (FSCC) to reach osmotic equilibrium with the externally imposed 1 bar of H_2 at 350 °C, 300 °C, 250 °C, 200 °C, 150 °C, and 100 °C, respectively, and H_2 pressures inside a FSCC was very close to the externally imposed values after osmotic equilibrium. By using FSCC as a hydrogen fugacity sensor, equilibrium H_2 pressures for Ni-NiO-H_2O and Co-CoO-H_2O redox buffer assemblages at 250–400 °C and 1000 bar total pressure were measured. The equilibrated f_{O_2} calculated are consistent with those derived from previous literatures. Besides, FSCC can also be used as a sample container, where f_{H_2} and f_{O_2} of enclosed samples can be continuously controlled. Furthermore, FSCC is an ideal container for sulfur-bearing samples and its transparency allows spectroscopic analyses of the sample. Our work extended the low-*T* limit of previously well-developed redox control techniques and may open up a new research avenue in low-*T* hydrothermal experiments.

Keywords: Redox buffer and control techniques; hydrothermal experiments; redox reactions; hydrogen fugacity sensor; fused silica capillary

This is the peer-reviewed, final accepted version for American Mineralogist, published by the Mineralogical Society of America.
The published version is subject to change. Cite as Authors (Year) Title. American Mineralogist, in press.
DOI: https://doi.org/10.2138/am-2021-7687. http://www.minsocam.org/

Introduction

Double-capsule (or oxygen buffer; Eugster 1957) and Shaw membrane (Shaw 1963) techniques are commonly applied to control f_{O_2} in hydrothermal experiments at elevated pressure-temperature (*P*-*T*) conditions (normally > 50 MPa and 600 °C). The success of these two techniques relies on the effective diffusion of hydrogen across hydrogen membranes (e.g., Pt or Ag-Pd alloys), which are commonly used as the sample container. The oxygen buffer technique defines f_{O_2} by the equilibrium reaction between solid buffer assemblages (e.g., Ni-NiO) and H_2O, while the Shaw membrane technique defines f_{O_2} by a hydrogen reservoir with known H_2 partial pressure. Over approximately the last 60 years, these two techniques have been greatly refined and widely used in hydrothermal experiments (Chou 1987; Scaillet et al. 1992; Taylor et al. 1992; Schmidt et al. 1995; Berndt et al. 2002; Matthews et al. 2003; Alex and Zajacz 2020).

However, double-capsule and Shaw membrane techniques do not work efficiently at *T* below 450 °C, as the permeability of commonly used precious metal hydrogen membranes to H_2 may become too low to achieve osmotic equilibrium between the sample system and the buffer/reservoir system in a reasonable duration (Chou 1986). Pd-rich Ag-Pd and Au-Pd alloys were tested to have high permeability to H_2 at low-*T* (e.g., Gunter 1987; Sonwane et al. 2006). Nevertheless, a relatively long experimental duration is still needed for Pd-rich alloys to achieve H_2 osmotic equilibrium at low-*T* (e.g., 5 days at 300 °C; Chou 1989) and they cannot be employed in sulfur-bearing studies. As a consequence, f_{O_2} conditions in hydrothermal experiments performed at *T* below 450 °C has normally been defined through: (1) mixing a solid oxygen buffer together with studied samples without a hydrogen membrane separating them (e.g., Gibert et al. 1998; Seewald 2001; Tagirov et al. 2005; Kokh et al. 2017); (2) loading a solid

67 oxygen buffer into a quartz tube holder that is immersed in the sample solution in an autoclave
68 with the open end exposed to the vapor phase of the sample (e.g., Archibald et al. 2001;
69 Timofeev et al. 2018); and (3) redox equilibrium of aqueous multivalent-element species (e.g.,
70 sulfur; Pokrovski et al. 2015; Kokh et al. 2020). However, above-mentioned methods may suffer
71 from leakage of H_2 from the autoclave and possibly slow reaction kinetics of the redox buffer at
72 low *T*. Therefore, it is necessary to develop a hydrogen fugacity sensor for directly monitoring
73 the actual sample f_{H_2} (or f_{O_2}) in low-*T* (< 450 ºC) hydrothermal experiments.

74 Diffusion coefficient measurements (Shang et al. 2009) demonstrated that fused silica is
75 highly permeable to H_2 even at *T* below 400 °C. For example, the diffusion coefficient of H_2 in
76 fused silica at 200 °C ($10^{-12.9}$ m^2/s) is two orders of magnitude higher than that in Pt at 600 °C
77 ($10^{-14.9}$ m^2/s; Chou 1986). In addition, the transparency of fused silica enables phase
78 observations and spectroscopic analyses for samples in a fused silica capillary capsule (FSCC).
79 The composition and internal pressure (density) of fluid samples inside an FSCC can be
80 determined by non-destructive spectroscopic methods (e.g., Raman spectroscopy; Chou et al.
81 2008). These characteristics make fused silica a potential hydrogen membrane, and FSCC a
82 suitable hydrogen fugacity senor and reactor for low-*T* hydrothermal experiments.

83 In this study, we first evaluated the viability of using fused silica as a low-*T* hydrogen
84 membrane and then demonstrated that redox conditions in low-*T* hydrothermal experiments can
85 be monitored and controlled by using FSCC as hydrogen fugacity sensor and reactor.

86

87

88

This is the peer-reviewed, final accepted version for American Mineralogist, published by the Mineralogical Society of America.
The published version is subject to change. Cite as Authors (Year) Title. American Mineralogist, in press.
DOI: https://doi.org/10.2138/am-2021-7687. http://www.minsocam.org/

Methods

Experimental apparatus

Fused silica capillary capsule (FSCC). FSCC was constructed from a fused silica capillary tubing with two ends sealed (Fig. 1; Chou et al. 2008). A FSCC can be loaded with solid, liquid or gaseous sample and also can be vacuumed (Chou et al. 2008). Two types of FSCC, *i.e.*, CO_2-FSCC and vacuumed FSCC, were used in present study. CO_2-FSCC contains a certain amount of CO_2 whereas vacuumed FSCC is internally vacuumed. Both CO_2- and vacuumed FSCC are normally ~10 mm long and have round cross sections with 0.1 mm inner diameter (ID) and 0.375 mm outer diameter (OD). Details about construction and sample-loading methods for FSCC are given in Chou et al. (2008).

Cold-sealed pressure vessel (CSPV). All experiments were carried out in horizontal CSPVs. Samples were normally loaded in a gold capsule (4.0 mm ID, 4.4 mm OD and ~3 cm long) and then placed into a CSPV, followed by a stainless steel filler rod (~20 cm long). The sample in the CSPV was heated by a horizontal electric furnace, and the sample *T* was monitored by using a K-type thermocouple, which was inserted into an external borehole of the CSPV near the sample. The accuracy of the reported temperature is within ± 3 °C, and the maximum temperature difference along the ~3 cm-long sample is less than 3 °C. At the conclusion of heating, the CSPV was quenched in a compressed air jet, and the temperature of the sample decreased to near room *T* within 5 minutes.

Experimental design

Experimental design of present study was summarized in Table 1, and details about experimental runs were given in Supplemental Table S1. Three sets of experiments were conducted. The first set of experiments (Set-I) determined the experimental durations required

for the sample fluid in a FSCC to reach osmotic equilibrium with externally imposed 1 bar of H_2 at T between 100 and 350 °C. We used two CO_2-FSCCs for each test: one contained ~1 bar of CO_2 (CO_2-FSCC-A), and the other contained ~0.5 bar (CO_2-FSCC-B). CO_2 was used as an internal reference in Raman analyses of H_2 and, due to the strong kinetic barriers, chemical reactions between H_2 and CO_2 are negligible in our experimental P-T conditions (< 400 °C; McCollom 2016). The CO_2-FSCCs were heated in a cold-sealed pressure vessel (CSPV) at a desired T under 1 bar of external H_2 P (Fig. 1) for a certain period of duration before quenching. Raman spectra of CO_2 and H_2 in the quenched CO_2-FSCCs were then collected, and the peak height ratios (HR) of H_2 and CO_2 of specific Raman bands were calculated.

The second set of experiments (Set-II) quantitatively determined the actual H_2 pressures in FSCCs after they reached osmotic equilibrium with externally imposed 1.5, 1.0 and 0.5 bar of H_2 at 200–350 °C. For each run, three vacuumed FSCCs were loaded into a CSPV and imposed with pure H_2 at a fixed P ($(P_{H_2})_{CSPV}$ = 1.5, 1.0 or 0.5 bar) before being heated at a fixed T (350, 300, 250 or 200 °C; Fig. 1). After the vacuumed FSCCs were heated for durations that are enough for reaching hydrogen osmotic equilibria (based on results in Set-I), they were then quenched, and the hydrogen P in each of them were determined at room T ($(P_{H_2})_{RT}$; see Analysis and calculation methods). The hydrogen P at an experimental T, $(P_{H_2})_T$, was calculated from the measured $(P_{H_2})_{RT}$ based on the ideal gas law (see Analysis and calculation methods).

In the third sets of experiments (Set-III), we determined equilibrated hydrogen fugacity ($(f_{H_2})_{P,T}$) and oxygen fugacity ($(f_{O_2})_{P,T}$) defined by Co-CoO-H_2O and Ni-NiO- H_2O buffer assemblages at 1000 bar and 250–400 °C. In these experiments, three or four vacuumed FSCCs, together with a solid oxygen buffer and H_2O, were sealed in a gold capsule (Fig. 2) and then pressurized with Ar in a CSPV before being heated to a desired P-T condition. During the

experiments, H_2 produced by the reaction between the oxygen buffer and H_2O diffused into the vacuumed FSCCs (Fig. 2). After osmotic and chemical equilibria were reached, $(f_{H_2})_{P,T}$ defined by the redox buffer at the experimental *P*-*T* is equal to those in the vacuumed FSCCs, and can be calculated from the measured $(P_{H_2})_{RT}$ in the quenched vacuumed FSCCs (see Analysis and calculation methods). Chemical regents used consist of Ni (99.99%, Aladdin Reagent), NiO (99.9%, Aladdin Reagent), Co (99.99%, Aladdin Reagent), CoO (99.5%, Aladdin Reagent) and deionized H_2O. In runs with Ni-NiO-H_2O or Co-CoO-H_2O as starting material, 40 mg H_2O and ~400 mg Ni-NiO or Co-CoO mixtures (mass ratio = 1:1) were used while for runs with Ni-H_2O or Co-H_2O as starting material, 40 mg H_2O and ~200 mg Ni or Co were used.

Raman spectra collection and treatment

Raman spectra were acquired with a JY/Horiba LabRAM HR Evolution Raman spectrometer using a 532.06 nm (Nd: YAG) laser, an SLWD 50x Olympus objective with 0.35 numerical aperture. 1800 groove/mm grating and 150 μm pinhole were used. The spectral resolution is approximately 0.2 cm^{-1}. The output laser power is 100 mW while ~14 mW of laser light was focused near the centre of the sample cell to generate Raman signals during measurements.

In Set-I experiments, Raman spectra of the two quenched CO_2-FSCCs between 300 and 1500 cm^{-1}, which covers four rational bands of H_2 and two Fermi diad of CO_2, were collected with 100s acquisition time, twice accumulations. For recovered vacuumed FSCCs from Set-II and Set-III experiments, Raman spectra in range of 4100–4200 cm^{-1}, which covers the four vibrational bands of H_2, were collected. The acquisition time is 100s or 200s with twice accumulations.

This is the peer-reviewed, final accepted version for American Mineralogist, published by the Mineralogical Society of America.
The published version is subject to change. Cite as Authors (Year) Title. American Mineralogist, in press.
DOI: https://doi.org/10.2138/am-2021-7687. http://www.minsocam.org/

Raman peak heights of $S_0(1)$ band (~588 cm^{-1}) of H_2, upper band of Fermi diad of CO_2 (~1388 cm^{-1}) and $Q_1(1)$ band of H_2 (~4157 cm^{-1}) were calculated from acquired spectra by using GRAM32/AI software. No smoothing or baseline correction was applied to the spectra and a liner baseline, which is close to mean of background (noise) signals, was manually defined during peak height acquisition (Fig. 3). It is worth noting that peak height, instead of peak area, was employed in quantitative analysis in present study. This is because pressure of H_2 in FSCCs is generally low (< 1.5 bar), so that the acquired H_2 spectra are normally not in good quality for conducting precise peak area calculations, while peak height can be calculated more easily and accurately.

Analysis and calculation methods

Determination of $(P_{H_2})_{RT}$ and $(P_{H_2})_T$ in vacuumed FSCCs. The pressure of H_2 in a quenched vacuumed FSCC at room T, $(P_{H_2})_{RT}$, was determined through a quantitative Raman spectroscopic analysis method. In this method, the quantitative relationships between the peak height of H_2 and its pressure were experimentally established. $(P_{H_2})_{RT}$ was then calculated from the acquired H_2 peak height, $(PH_{H_2})_{RT}$, based on the established quantitative relationships (details see Appendix A).

Because of the low pressures (< 1.5 bar) of H_2 in vacuumed FSCCs, H_2 gas in an individual vacuumed FSCC can be treated as an ideal gas both at room T and experimental T. Considering the low thermal expansion coefficient of fused silica (5.5×10^{-7} K^{-1}; Deng et al. 2020), the volume of each vacuumed FSCC can be treated as a constant during experiments and assume no H_2 loss from the equilibrated FSCCs during and after quenching. We obtain:

This is the peer-reviewed, final accepted version for American Mineralogist, published by the Mineralogical Society of America.
The published version is subject to change. Cite as Authors (Year) Title. American Mineralogist, in press.
DOI: https://doi.org/10.2138/am-2021-7687. http://www.minsocam.org/

$$\left(P_{H_2}\right)_T = \left(P_{H_2}\right)_{RT} \frac{T}{T_{room}} \quad (1)$$

where $(P_{H_2})_{RT}$ and $(P_{H_2})_T$ are the pressures of H_2 in a vacuumed FSCC at room T and experimental T, respectively. T is in K, and T_{room} is equal to 298.15 K.

$(f_{H_2})_{P,T}$, $(f_{O_2})_{P,T}$ and $(f_{O_2})_{1,T}$ calculation. As an ideal gas, the fugacity of the H_2 in a vacuumed FSCC at an experimental P-T ($(f_{H_2})_{P,T}$) is equal to its H_2 pressure $(P_{H_2})_T$:

$$\left(f_{H_2}\right)_{P,T} = \left(P_{H_2}\right)_T \quad (2)$$

For the formation reaction of H_2O,

$$H_{2(g)} + 0.5\ O_{2(g)} = H_2O_{(g)} \quad (3)$$

$$\log K_w = \log f_{H_2O} - \log f_{H_2} - 0.5 \log f_{O_2} \quad (4)$$

where K_w is the formation constant of H_2O at T and f_{H_2O} is the fugacity of H_2O at P and T. Because both K_w and f_{H_2O} at P and T are well known (Burnham et al. 1969), log f_{O_2} at P and T (log $(f_{O_2})_{P,T}$) can be calculated from $(f_{H_2})_{P,T}$ based on Eq. (4), where $(f_{H_2})_{P,T}$ is calculated from measured $(P_{H_2})_{RT}$ based on Eqs. (1) and (2). The obtained $(f_{O_2})_{P,T}$ value is related to f_{O_2} at one bar and T ($(f_{O_2})_{1,T}$) as:

$$\log \left(f_{O_2}\right)_{1,T} = \log \left(f_{O_2}\right)_{P,T} + \frac{\Delta V (P-1)}{2.303RT} \quad (5)$$

where T is in K, P is in bar, R is the gas constant (8.314 J·mol^{-1}·K^{-1}), and ΔV is the volume change for the solid phases in the buffer reaction and was calculated using molar volume data from Robie and Hemingway (1995).

The limit of detection (LOD) and limit of quantitation (LOQ) for the H_2 in vacuumed FSCCs at room T are estimated to be 0.02 bar and 0.06 bar, respectively (details see Appendix B). The

uncertainties in $(P_{H_2})_{RT}$, $(f_{O_2})_{P,T}$ and $(f_{O_2})_{1,T}$ were calculated based on the method described in Appendix C.

Results and discussion

Fused silica as a low-*T* (< 450 °C) hydrogen membrane

Fig. 3 shows Raman spectra collected from a quenched CO_2-FSCC after it was heated at 250 °C, under 1 bar external H_2 for various experimental durations (Set-I experiments). The peak height ratios between H_2 and CO_2 (*HR*) were derived from $S_0(1)$ Raman band (near 588 cm^{-1}) of H_2 and the upper band of CO_2 Fermi diad (near 1388 cm^{-1}). As shown in Fig. 3, *HR* value increases with experimental duration at first (from 4 to12 hrs) and then remains almost unchanged (from 16 to 24 hrs), indicating the initial flux of H_2 into the CO_2-FSCC until it reached osmotic equilibrium with the externally imposed 1 bar H_2. This *HR vs.* experimental duration trend was observed for all CO_2-FSCCs used in Set-I experiments (Fig. 4; Supplemental Table S2). The experimental duration at which *HR* begins to level off represents the minimum duration required for a FSCC to achieve osmotic equilibrium with 1 bar H_2 at a specific *T*. Results show that 3, 8, 16, 36, 96, 216 hours are required for a FSCC to attain such equilibrium at 350, 300, 250, 200, 150 and 100 °C, respectively (Fig. 4).

Results of Set-II experiments were shown in Fig. 5 and tabulated in Supplemental Table S3. Each $(P_{H_2})_{RT}$ value given is the average of three data derived from three Raman spectra collected at three different locations of a single quenched vacuumed FSCC. The hydrogen *P* at experimental *T*, $(P_{H_2})_T$, was calculated from the measured $(P_{H_2})_{RT}$ based on Eq. (1). ΔP_{H_2} is the

219 difference between $(P_{H_2})_T$ and $(P_{H_2})_{CSPV}$ ($\Delta P_{H_2} = (P_{H_2})_T - (P_{H_2})_{CSPV}$). The results show that
220 $(P_{H_2})_T$ is near the externally imposed $(P_{H_2})_{CSPV}$ (Fig. 5).

221 These two sets (I and II) of experiments verified that fused silica can serve effectively as a
222 low-*T* hydrogen membrane at least down to 200 °C: it reaches H_2 osmotic equilibrium very
223 quickly at these low *T*s, and the H_2 pressure determined in V-FSCCs were very close to the
224 externally imposed value, without hydrogen pressure lag existing (Hewitt, 1977).

225 **Redox measurement or monitoring in low-*T* hydrothermal experiments**

226 Redox measurement or monitoring in low-*T* hydrothermal experiments can be achieved by
227 using a vacuumed FSCC as a hydrogen fugacity sensor. As an example, the f_{H_2} and f_{O_2} defined
228 by Co-CoO and Ni-NiO buffers at 1000 bar and 250–400 °C were determined. The results show
229 that equilibria between the studied solid oxygen buffers and H_2O can be reached within 24 hours
230 at *T* between 250–400 °C, and steady $(f_{O_2})_{P,T}$ values were always present at each experimental *T*
231 after reaching equilibrium (Figs. 6, 7; Supplemental Tables S4, S5). The log $(f_{O_2})_{1,T}$ values
232 derived from measured $(P_{H_2})_{RT}$ agree well with those retrieved from thermochemical data and
233 previous literature (Fig. 8; Table 2).

234 The thermochemical and kinetic properties of solid oxygen buffers at elevated *P*-*T* conditions
235 (> 600 °C) have been extensively studied. However, these properties have rarely been
236 experimentally measured at low *Ts* (< 450 °C); Burkhard and Ulmer (1995) evaluated the
237 thermodynamic properties of several solid oxygen buffers at *Ts* down to 300 °C at 1 atm in a dry
238 system using a ZrO_2 oxygen sensor, and Kishima and Sakai (1984) and Lemke et al. (2008)
239 measured f_{O_2}-*T* relationships of several solid buffers at a low *T* range (300–500 °C) in a
240 Dickson-type autoclave. Our experiments mimicked a realistic oxygen-buffering scenario and

confirmed that equilibrium between solid buffers and H_2O can be reached quickly at low *T*, with steady and reproducible equilibrated f_{O_2} values achieved at each experimental *T*. Therefore, we verified that the solid buffers can also be used to control f_{O_2} in relatively low-*T* hydrothermal experiments. However, considering that the leakage of H_2 through the autoclave and the exhaustion of the redox buffer may happen during hydrothermal experiments, it is advisable to use a low-*T* redox sensor (a vacuumed FSCC, for instance) to directly measure the actual redox state of an experiment.

Redox control in low-*T* hydrothermal experiments

FSCC can be used as a sample container for low-*T* hydrothermal experiments, where f_{H_2} and f_{O_2} can be continuously controlled. The f_{H_2} of samples sealed in FSCCs can be easily controlled by letting the FSCCs equilibrate with an externally imposed H_2 pressure in a CSPV at a given experimental *T* (Fig. 1). However, unlike a flexible Pt or Ag-Pd alloy capsule, FSCC is rigid, such that pressure cannot be transmitted from the external pressure medium into the sealed samples, and thus, f_{H_2O}, as well as f_{O_2}, of the samples cannot be easily controlled. Nonetheless, provided that there is always a coexisting vapor phase during an experiment, the studied sample will always be under vapor-saturated water pressures during the experiment. In this case, f_{H_2O} will be fixed at the specific experimental *T* (in K) by the following equation (Giggenbach, 1980):

$$\log f_{H_2O} = 5.510 - \frac{2048}{T} \quad (6)$$

Therefore, the f_{O_2} of the studied sample sealed in an FSCC can be defined by the externally imposed H_2 *P* through the formation constant of H_2O.

Implications

The new redox control and measurement technique presented here effectively extends the conventional double-capsule (or oxygen buffer) and Shaw membrane techniques down to 200 °C, and the new technique also has its own advantages: (1) the volumes of FSCCs (n × 10^{-3} mm^3) are much smaller than those of Pt or Ag-Pd alloy capsules (n × 10^2 mm^3) and therefore a much shorter time is required to reach osmotic equilibrium; (2) the composition of studied samples before and after experiments can be directly measured by using Raman spectroscopic method; (3) the experimental setup is relatively simple without complex welding and soldering work; (4) dozens of FSCCs loaded with various samples can be heated to the desired T and P_{H_2} conditions at the same time; and (5) FSCCs can be used to study geologically important sulfur-bearing systems because they are inert to sulfur. This new technique has broad prospects for hydrothermal experiments conducted in the low-T regime.

Acknowledgments and Funding

We thank Dr. Y. Wan, Ms. Y. Chen, Ms. H.Y. Zhang, Mr. M.K. Hu and Mr. R.H. Wang in the Institute of Deep-sea Science and Engineering, Chinese Academy of Sciences for their assistance in our experiments. Discussions with Prof. L.B. Shang in the Institute of Geochemistry, Chinese Academy of Sciences improved our experimental design. Results presented here were mostly taken from JF's Ph.D. dissertation submitted to University of Chinese Academy of Sciences. This study was funded by the Key Frontier Science Program (QYZDY-SSW-DQC008) of Chinese Academy of Sciences, and (Chinese) National Natural Science Foundation (No. 41973055).

References Cited

283 Alex, A. and Zajacz, Z. (2020) A new method to quantitatively control oxygen fugacity in
284 externally heated pressure vessel experiments. European Journal of Mineralogy, 32, 219–
285 234.
286 Archibald, S.M., Migdisov, A.A. and Williams-Jones, A.E. (2001) The stability of Au-chloride
287 complexes in water vapor at elevated temperatures and pressures. Geochimica et
288 Cosmochimica Acta, 65, 4413–4423.
289 Berndt, J., Liebske, C., Holtz, F., Freise, M., Nowak, M., Ziegenbein, D., Hurkuck, W. and
290 Koepke, J.r. (2002) A combined rapid-quench and H_2-membrane setup for internally heated
291 pressure vessels: Description and application for water solubility in basaltic melts.
292 American Mineralogist, 87, 1717–1726.
293 Burnham, C.W., Holloway, J.R. and Davis, N.F. (1969) Thermodynamic Properties of Water to
294 1000 °C and 10000 Bars. Geological Society of America Special Papers, 132, 1–96.
295 Burkhard, D. J. M. and Ulmer, G. C. (1995) Kinetics and equilibria of redox systems at
296 temperatures as low as 300°C. Geochimica et Cosmochimica Acta, 59, 1699–1714.
297 Chou, I.M. (1986) Permeability of precious metals to hydrogen at 2 kb total pressure and
298 elevated temperatures. American Journal of Science, 286, 638–658.
299 Chou, I.M. (1987) Oxygen buffer and hydrogen sensor techniques at elevated pressures and
300 temperatures. In G.C. Ulmer and H. L. Barnes, Eds., Hydrothermal experimental techniques,
301 p. 61–99. John Wiley and Sons, New York.
302 Chou, I.M. (1989) A low-temperature redox sensor. EOS, 70, 507.
303 Chou, I.M., Song, Y. and Burruss, R. C. (2008) A new method for synthesizing fluid inclusions
304 in fused silica capillaries containing organic and inorganic material. Geochimica et
305 Cosmochimica Acta, 72, 5217–5231.

306 Deng, B., Shi, Y. and Yuan, F. (2020) Investigation on the structural origin of low thermal
307 expansion coefficient of fused silica. Materialia, 12, 100752.
308 Eugster, H. P. (1957) Heterogeneous reactions involving oxidation and reduction at high
309 pressures and temperatures. The Journal of Chemical Physics, 26, 1760–1761.
310 Gibert, F., Pascal, M.L. and Pichavant, M. (1998) Gold solubility and speciation in hydrothermal
311 solutions: Experimental study of the the stability of hydrosuphide complex of gold ($AuHS^0$)
312 at 350 to 450 ºC and 500 bars. Geochimica et Cosmochimica Acta, 62, 2931–2947.
313 Giggenbach, W. F. (1980) Geothermal gas equilibria. Geochimica et Cosmochimica Acta, 44,
314 2021–2032.
315 Gunter, M., Myers, J. and Girsperberg,S. (1987) Hydrogen: metal membranes. In G.C. Ulmer
316 and H. L. Barnes, Eds., Hydrothermal experimental techniques, p. 100–120. John Wiley and
317 Sons, New York.
318 Hewitt, D.A. (1977) Hydrogen fugacities in Shaw bomb experiments. Contributions to
319 Mineralogy and Petrology, 65, 165–169.
320 Huebner, J. S. and Sato, M. (1970) The oxygen fugacity-temperature relationships of manganese
321 oxide and nickel oxide buffers. American Mineralogist, 55, 934–952.
322 Kishima, N. and Sakai, H. (1984) A simple gas analytical technique for the Dickson-type
323 hydrothermal apparatus and its application to the calibration of MH, NNO and FMQ oxygen
324 buffers. Geochemical Journal. 18, 19–29.
325 Kokh, M.A., Akinfiev, N.N., Pokrovski, G.S., Salvi, S. and Guillaume, D., 2017. The role of
326 carbon dioxide in the transport and fractionation of metals by geological fluids. Geochimica
327 et Cosmochimica Acta 197, 433–466.

328 Kokh, M.A., Assayag, N., Mounic, S., Cartigny, P., Gurenko, A. and Pokrovski, G.S., 2020.
329 Multiple sulfur isotope fractionation in hydrothermal systems in the presence of radical ions
330 and molecular sulfur. Geochimica et Cosmochimica Acta 285, 100–128.
331 Lemke, K.H., Rosenbauer, R.J. Bischoff, J.L. and Bird, D.K. (2008) An hydrothermal
332 experimental study of the cobalt–cobalt oxide redox buffer. Chemical Geology, 252, 136–
333 144.
334 Matthews, W., Linnen, R.L. and Guo, Q. (2003) A filler-rod technique for controlling redox
335 conditions in cold-seal pressure vessels. American Mineralogist, 88, 701–707.
336 McCollom, T.M. (2016) Abiotic methane formation during experimental serpentinization of
337 olivine. Proceedings of the National Academy of Sciences, 113, 13965–13970.
338 O'Neill, H. S. C. and Pownceby, M. I. (1993) Thermodynamic data from redox reactions at high
339 temperatures. I. An experimental and theoretical assessment of the electrochemical method
340 using stabilized zirconia electrolytes, with revised values for the Fe-"FeO", Co-CoO, Ni-
341 NiO and Cu-Cu_2O oxygen buffers, and new data for the W-WO_2 buffer. Contributions to
342 Mineralogy and Petrology, 114, 296–314.
343 Pokrovski, G.S., Kokh, M.A., Guillaume, D., Borisova, A.Y., Gisquet, P., Hazemann, J.L.,
344 Lahera, E., Del Net, W., Proux, O. and Testemale, D. (2015) Sulfur radical species form
345 gold deposits on Earth. Proceedings of the National Academy of Sciences, 112, 13484–
346 13489.
347 Robie, R. A. and Hemingway, B. S. (1995) Thermodynamic properties of minerals and related
348 substances at 298.15 K and 1 Bar (10^5 Pascals) pressure and at higher temperatures. Bulletin
349 of the United States Geological Survey, 2131, 461.

350 Scaillet, B., Pichavant, M., Roux, J., Humbert, G. and Lefevre, A. (1992) Improvements of the
351 Shaw membrane technique for measurement and control of f_{H_2} at high temperatures and
352 pressures. American Mineralogist, 77, 647–655.
353 Schmidt, B., Scaillet, B. and Holtz, F. (1995) Accurate control of f_{H_2} in cold-seal pressure
354 vessels with the Shaw membrane technique. European Journal of Mineralogy, 7, 893–903.
355 Seewald, J.S. (2001) Aqueous geochemistry of low molecular weight hydrocarbons at elevated
356 temperatures and pressures: Constraints from mineral buffered laboratory experiemtnts.
357 Geochimica et Cosmochimica Acta, 95, 1641–1664.
358 Shaw, H. R. (1963) Hydrogen-water vapor mixtures: Control of hydrothermal atmospheres by
359 hydrogen osmosis. Science, 139, 1220–1222.
360 Shang, L., Chou, I.M., Lu W., Burruss, R.C. and Zhang, Y. (2009) Determination of diffusion
361 coefficients of hydrogen in fused silica between 296 and 523 K by Raman spectroscopy and
362 application of fused silica capillaries in studying redox reactions. Geochimica et
363 Cosmochimica Acta, 73, 5435–5443.
364 Sonwane, C.G., Wilcox, J. and Ma, Y.H. (2006) Achieving optimum hydrogen permeability in
365 PdAg and PdAu alloys. Journal of Chemical Physics, 125, 73–71.
366 Taylor, J.R., Wall, V. and Pownceby, M. (1992) The calibration and application of accurate
367 redox sensors. American Mineralogist, 77, 284–295.
368 Timofeev, A., Migdisov, A.A., Williams-Jones, A.E., Roback, R., Nelson, A.T. and Xu, H.
369 (2018) Uranium transport in acidic brines under reducing conditions. Nature
370 Communications. 9, 1469.

Tagirov, B.R., Salvi, S., Schott, J. and Baranova, N.N. (2005) Experimental study of gold-hydrosulphide complexing in aqueous solutions at 350–500 °C, 500 and 1000 bars using mineral buffers. Geochimica et Cosmochimica Acta, 69, 2119–2132.

Figure and Table captions

Figure 1. Experimental setup and procedures for Set-I and Set-II experiments. (a) Schematic diagram showing the experimental setup. (b) A one-end sealed gold capsule and five fused silica capillary capsules (FSCCs). (c) Two CO_2-FSCCs and three vacuumed FSCCs. CO_2-FSCCs contain ~0.5 or ~1.0 bar CO_2 while vacuumed FSCCs are internally vacuumed (c). In Set-I experiments, two CO_2-FSCCs were loaded in a gold capsule with one end open, which was in turn sealed and heated in a horizonal cold-sealed pressure vessel (CSPV), whereas, in Set-II experiments, three vacuumed FSCCs were used and loaded in the gold capsule. The CSPV was then evacuated and loaded with H_2, the pressure of which can be adjusted and monitored. H_2 at the set pressure was allowed to diffuse into the FSCCs at a fixed *T*.

Figure 2. A schematic diagram showing the capsule configuration for Set-III experiments. H_2, generated by the reaction of an oxygen buffer and H_2O in an enclosed gold capsule at a fixed *P*-*T* condition, diffused into vacuumed FSCCs. The ceramic tube is used to protect the FSCC when the external pressure is applied to the gold capsule. Modified from Fig. 14 of Chou et al. 2008.

Figure 3. Raman spectra collected from a quenched CO_2-FSCC after it was heated at 250 °C, under 1 bar H_2 external pressure for various experimental durations. Peak heights of H_2 (near 588

393 cm^{-1}) and CO_2 (near 1388 cm^{-1}) were acquired (showing in two insets), and their ratios, *HRs*,
394 were calculated and noted for each spectrum.

395 **Figure 4**. Diagrams showing the Raman peak height ratios between H_2 and CO_2 (*HR*) measured
396 in quenched CO_2-FSCCs (A and B) after they were exposed to 1 bar of H_2 external pressure at
397 350 °C (a), 300 °C (b), 250 °C (c), 200 °C (d), 150 °C (e) and 100 °C (f) for various durations.
398 The error bars represent the standard deviations and the horizontal dashed lines mark the
399 levelling off trends of *HR*.

400 **Figure 5**. Diagrams showing the results of Set-II experiments at 350 °C (a), 300 °C (b), 250 °C
401 (c) and 200 °C (d). Each solid circle represents a $(P_{H_2})_T$ value derived from measured $(P_{H_2})_{RT}$ in a
402 single vacuumed FSCC, and there were three vacuumed FSCCs in each experiment. Data for
403 $(P_{H_2})_{CSPV}$ = 1.5, 1.0 and 0.5 bar experiments are marked in blue, red and yellow, respectively.
404 The shaded areas represent ±0.1, ±0.1 and ±0.05 bar, respectively.

405 **Figure 6**. Values of $(P_{H_2})_{RT}$ measured as a function of experimental duration for Ni-NiO buffer
406 at 400 °C (a), 350 °C (b), 300 °C (c) and 250 °C (d). Plotted are the data listed in Supplemental
407 Table S4. Dashed lines mark the average $(P_{H_2})_{RT}$ values after equilibrium. Under each symbol,
408 the log $(f_{O_2})_{1,T}$ value calculated from the corresponding $(P_{H_2})_{RT}$ is shown. The starting materials
409 were Ni-H_2O (circles) and Ni-NiO-H_2O (squares).

410 **Figure 7**. Values of $(P_{H_2})_{RT}$ measured as a function of experimental duration for Co-CoO buffer
411 at 400 °C (a), 350 °C (b), 300 °C (c) and 250 °C (d). Plotted are the data listed in Supplemental
412 Table S4. Dashed lines mark the average $(P_{H_2})_{RT}$ values after equilibrium. Under each symbol,
413 the log $(f_{O_2})_{1,T}$ value calculated from the corresponding $(P_{H_2})_{RT}$ is shown. The starting materials
414 were Co-H_2O (circles) and Co-CoO-H_2O (squares).

415 **Figure 8**. Comparison of log $(f_{O_2})_{1,T}$ values obtained in this study at various temperatures with
416 previous data for Ni-NiO (a) and Co-CoO (b) buffers. The linear regression lines shown were
417 derived from the data listed in Table 2.

418 **Table 1**. Summary of experimental design

419 **Table 2**. Comparison of log $(f_{O_2})_{1,T}$ values for Ni-NiO and Co-CoO buffers derived from
420 measured H_2 pressures at room T in present study and those reported previously.

421

422

Figure 1

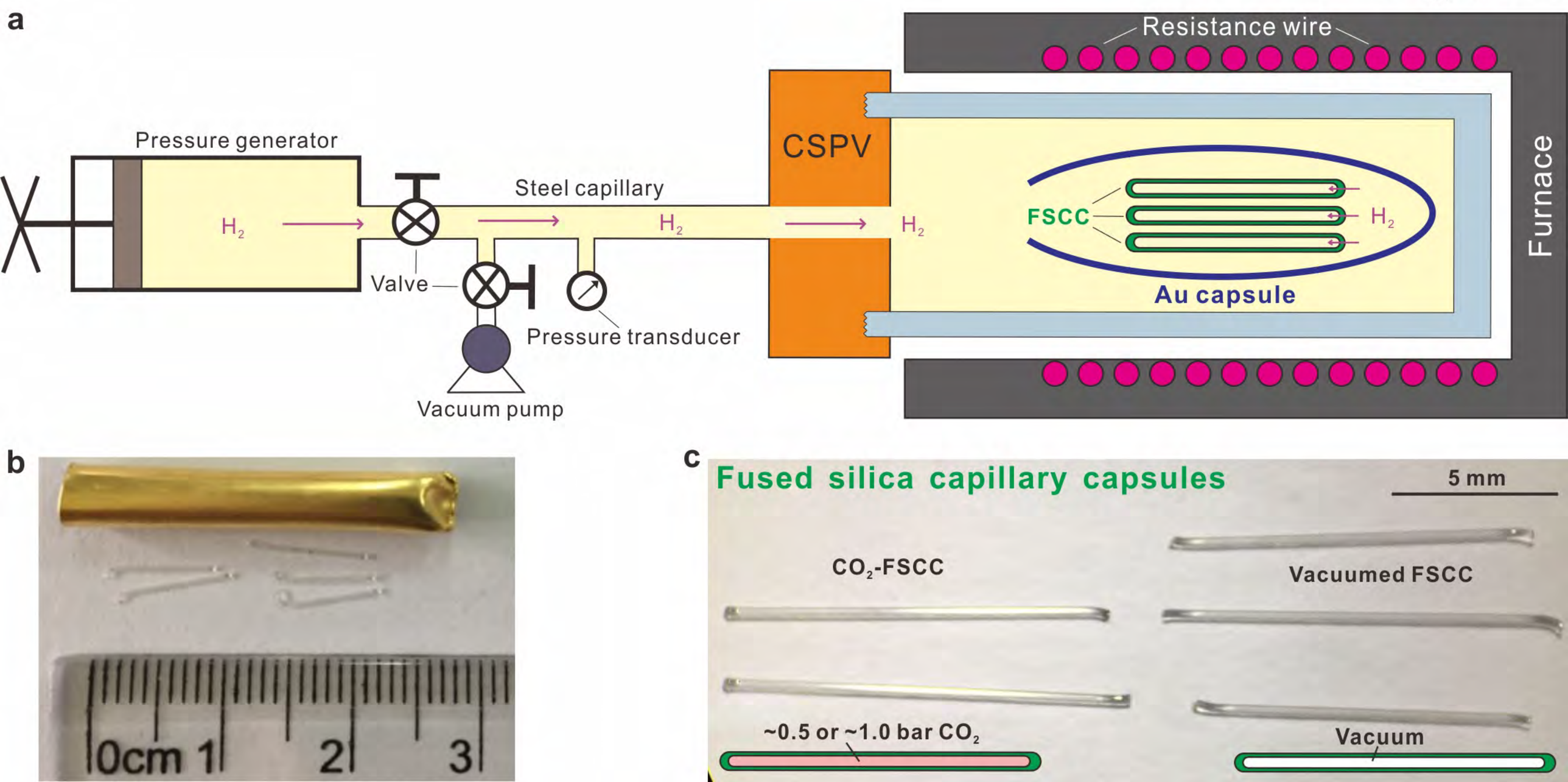
a
Resistance wire
Pressure generator
CSPV
Steel capillary
Furnace
H_2
H_2
H_2
H_2
FSCC
Valve
Au capsule
Pressure transducer
Vacuum pump
b
0cm 1 2 3
c
Fused silica capillary capsules
5 mm
CO_2-FSCC
Vacuumed FSCC
~0.5 or ~1.0 bar CO_2
Vacuum

Figure 2

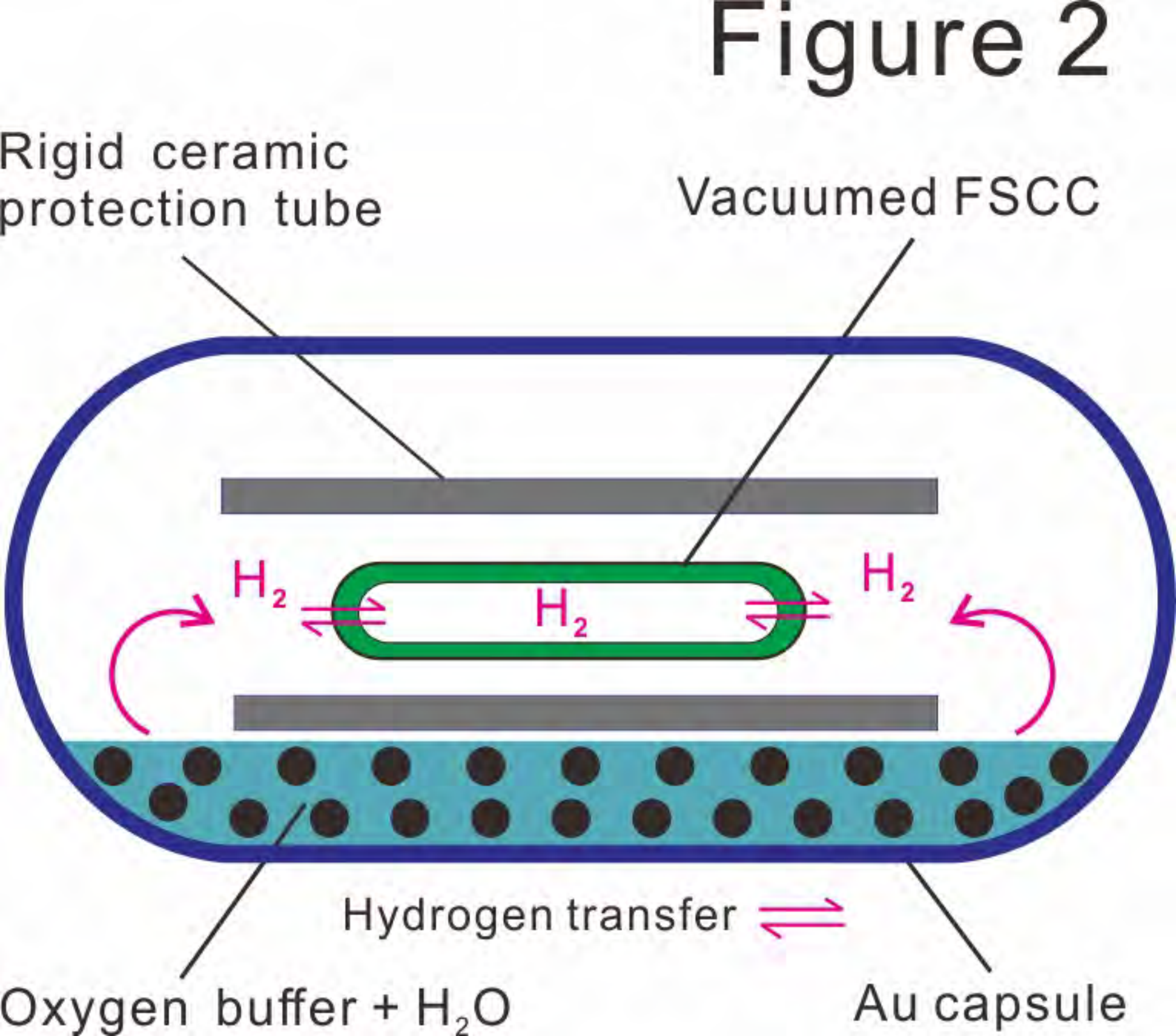
Rigid ceramic protection tube
Vacuumed FSCC
H_2
H_2
H_2
Hydrogen transfer
Oxygen buffer + H_2O
Au capsule

Figure 3

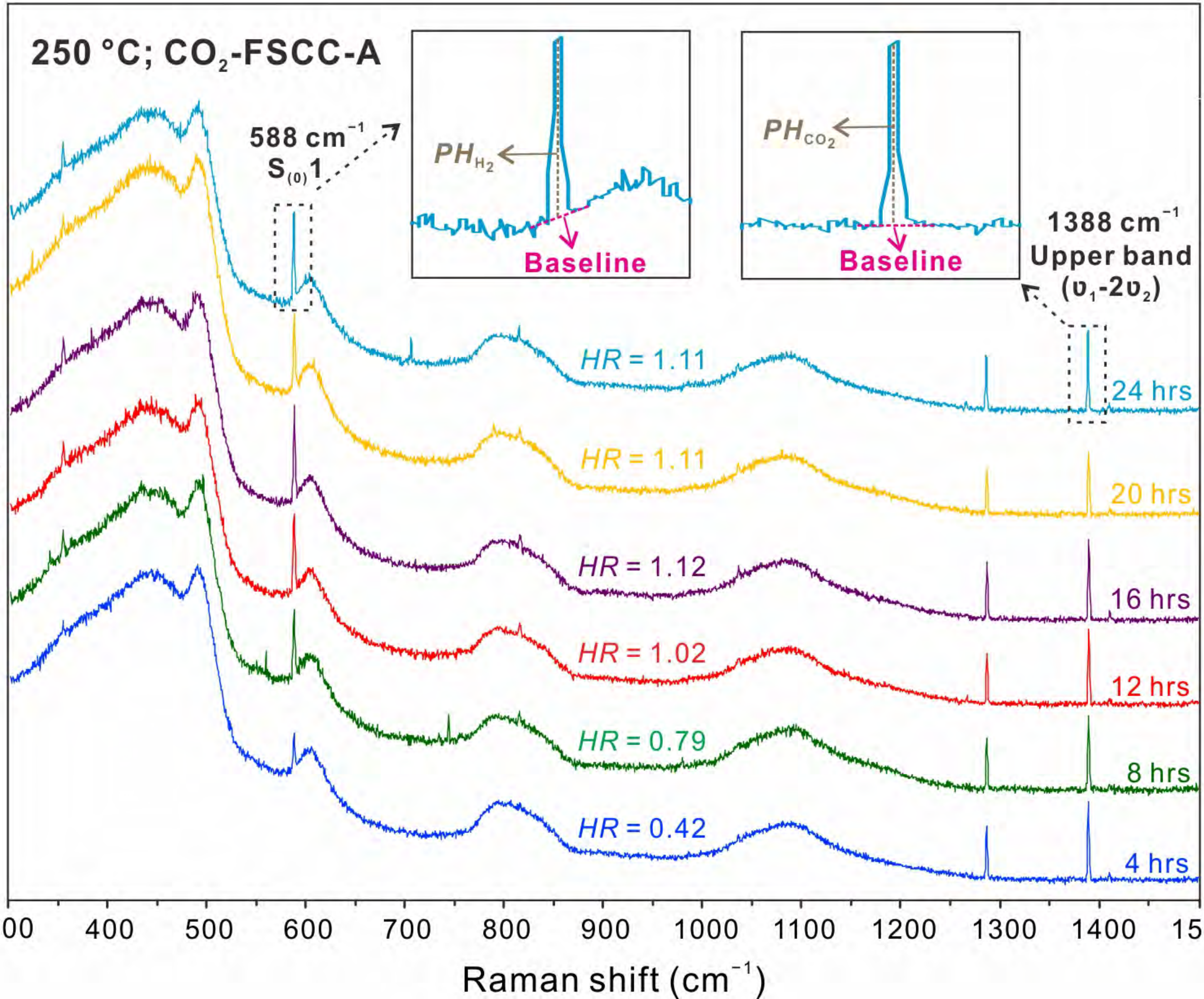
250 °C; CO2-FSCC-A
588 cm-1
S(0)1
PH H2
Baseline
PH CO2
Baseline
1388 cm-1
Upper band
(υ1-2υ2)
HR = 1.11
24 hrs
HR = 1.11
20 hrs
HR = 1.12
16 hrs
HR = 1.02
12 hrs
HR = 0.79
8 hrs
HR = 0.42
4 hrs
Intensity(a.u.)
300
400
500
600
700
800
900
1000
1100
1200
1300
1400
1500
Raman shift (cm-1)

Figure 4

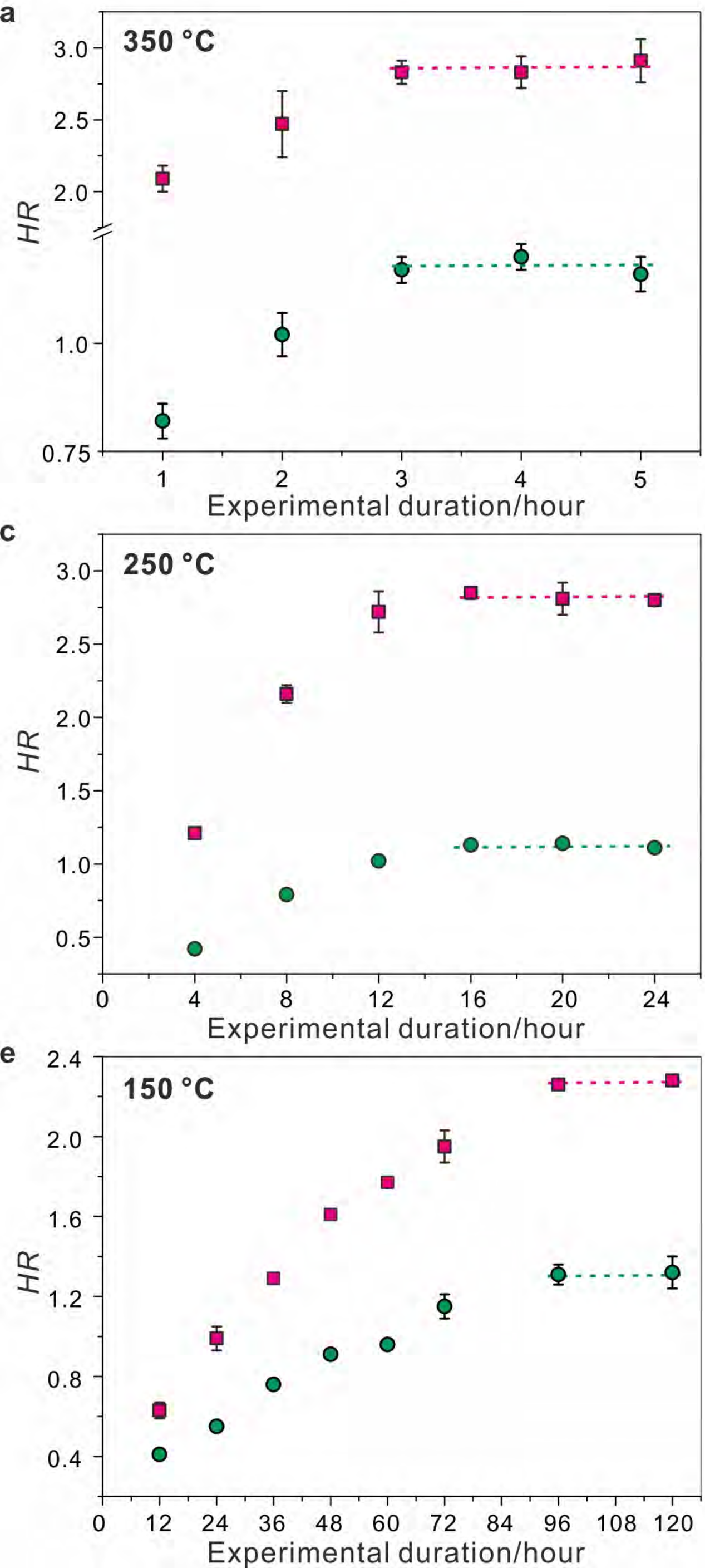
a
350 °C
HR
3.0
2.5
2.0
1.0
0.75
1
2
3
4
5
Experimental duration/hour
b
300 °C
HR
2.4
2.2
2.0
1.4
1.2
1.0
0.8
2
4
6
8
10
12
Experimental duration/hour
c
250 °C
HR
3.0
2.5
2.0
1.5
1.0
0.5
0
4
8
12
16
20
24
Experimental duration/hour
d
200 °C
HR
2.25
2.00
1.75
1.50
1.25
1.00
0.75
0.50
0.25
0
6
12
18
24
30
36
42
48
54
60
Experimental duration/hour
e
150 °C
HR
2.4
2.0
1.6
1.2
0.8
0.4
0
12
24
36
48
60
72
84
96
108
120
Experimental duration/hour
f
100 °C
HR
2.1
1.8
1.5
1.2
0.9
0.6
0.3
0
24
48
72
96
120
144
168
192
216
240
264
Experimental duration/hour
CO2-FSCC-A
CO2-FSCC-B

Figure 5

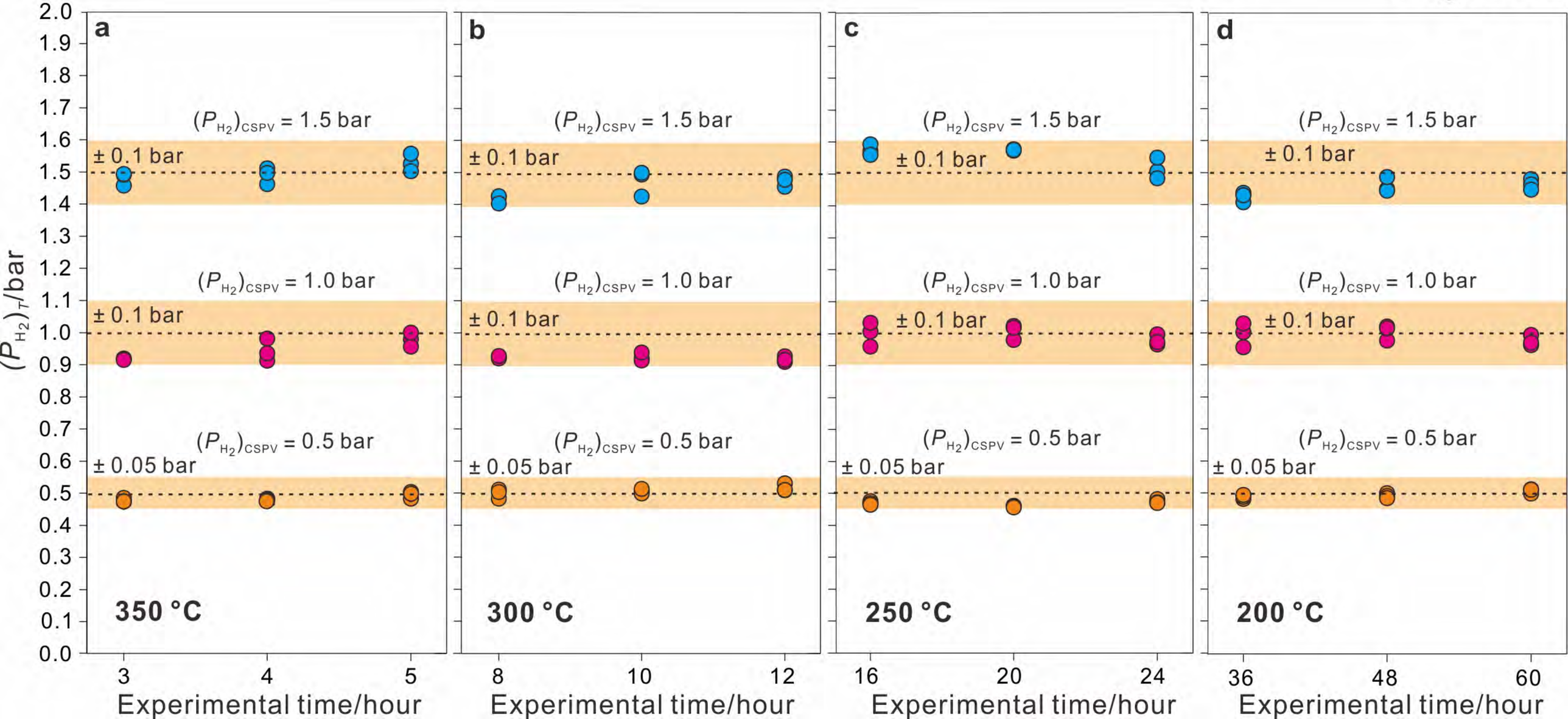
a
b
c
d
$(P_{H_2})_{CSPV}$ = 1.5 bar
± 0.1 bar
$(P_{H_2})_{CSPV}$ = 1.0 bar
± 0.1 bar
$(P_{H_2})_{CSPV}$ = 0.5 bar
± 0.05 bar
350 °C
300 °C
250 °C
200 °C
$(P_{H_2})_T$/bar
Experimental time/hour
2.0
1.9
1.8
1.7
1.6
1.5
1.4
1.3
1.2
1.1
1.0
0.9
0.8
0.7
0.6
0.5
0.4
0.3
0.2
0.1
0.0
3
4
5
8
10
12
16
20
24
36
48
60

Figure 6

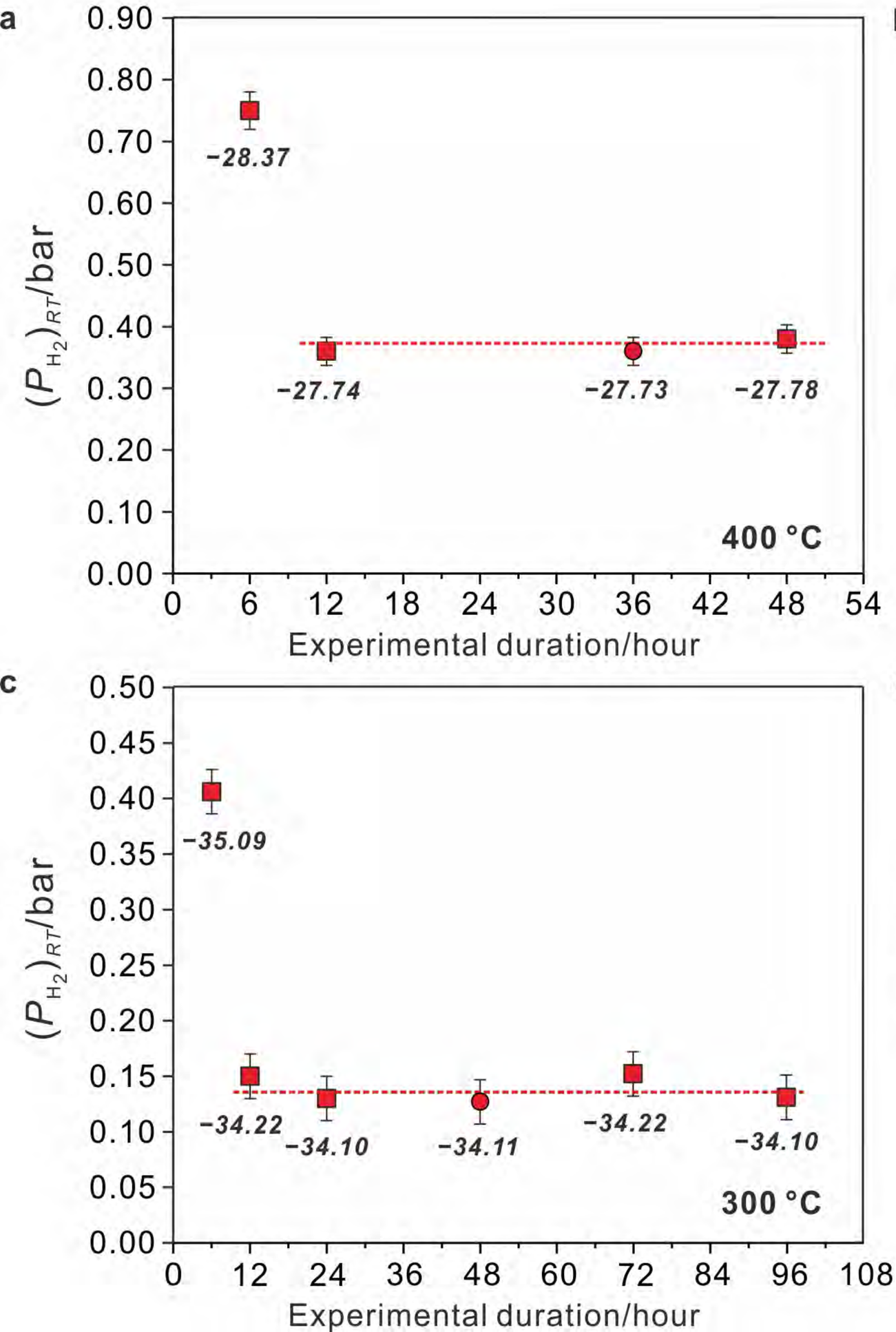
a
$(P_{H_2})_{RT}$/bar
0.00
0.10
0.20
0.30
0.40
0.50
0.60
0.70
0.80
0.90
0
6
12
18
24
30
36
42
48
54
Experimental duration/hour
−28.37
−27.74
−27.73
−27.78
400 °C
b
$(P_{H_2})_{RT}$/bar
0.00
0.05
0.10
0.15
0.20
0.25
0.30
0.35
0.40
0.45
0.50
0.55
0.60
0
12
24
36
48
60
72
84
96
108
Experimental duration/hour
−31.31
−30.75
−30.80
−30.87
−30.87
350 °C
c
$(P_{H_2})_{RT}$/bar
0.00
0.05
0.10
0.15
0.20
0.25
0.30
0.35
0.40
0.45
0.50
0
12
24
36
48
60
72
84
96
108
Experimental duration/hour
−35.09
−34.22
−34.10
−34.11
−34.22
−34.10
300 °C
d
$(P_{H_2})_{RT}$/bar
0.00
0.02
0.04
0.06
0.08
0.10
0.12
0.14
0.16
0.18
0.20
0
24
48
72
96
120
144
168
Experimental duration/hour
Ni-H_2O
Ni-NiO-H_2O
−38.39
−38.29
−38.30
−38.31
250 °C

Figure 7

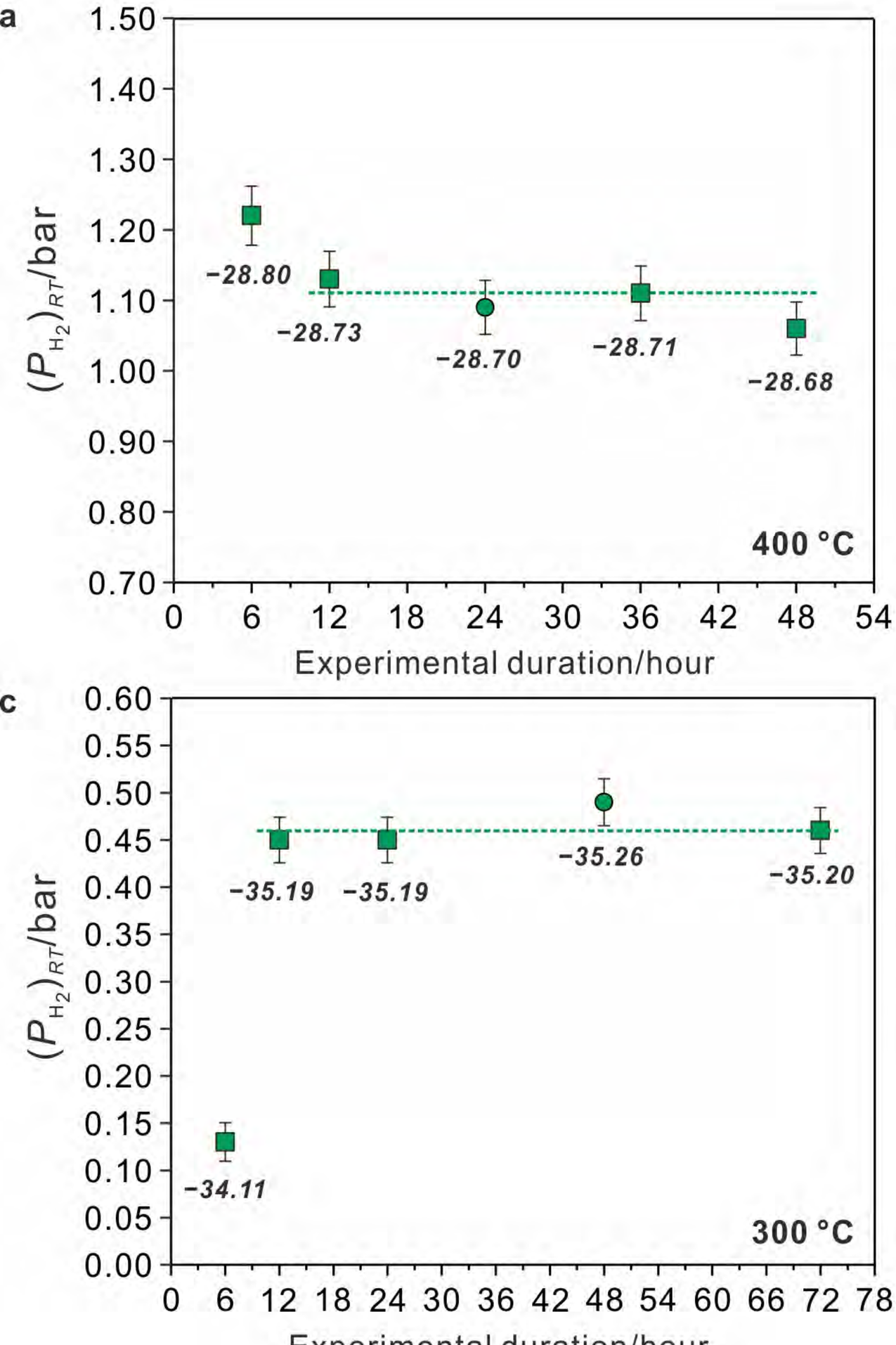
a
$(P_{H_2})_{RT}$/bar
1.50
1.40
1.30
1.20
1.10
1.00
0.90
0.80
0.70
−28.80
−28.73
−28.70
−28.71
−28.68
400 °C
0 6 12 18 24 30 36 42 48 54
Experimental duration/hour

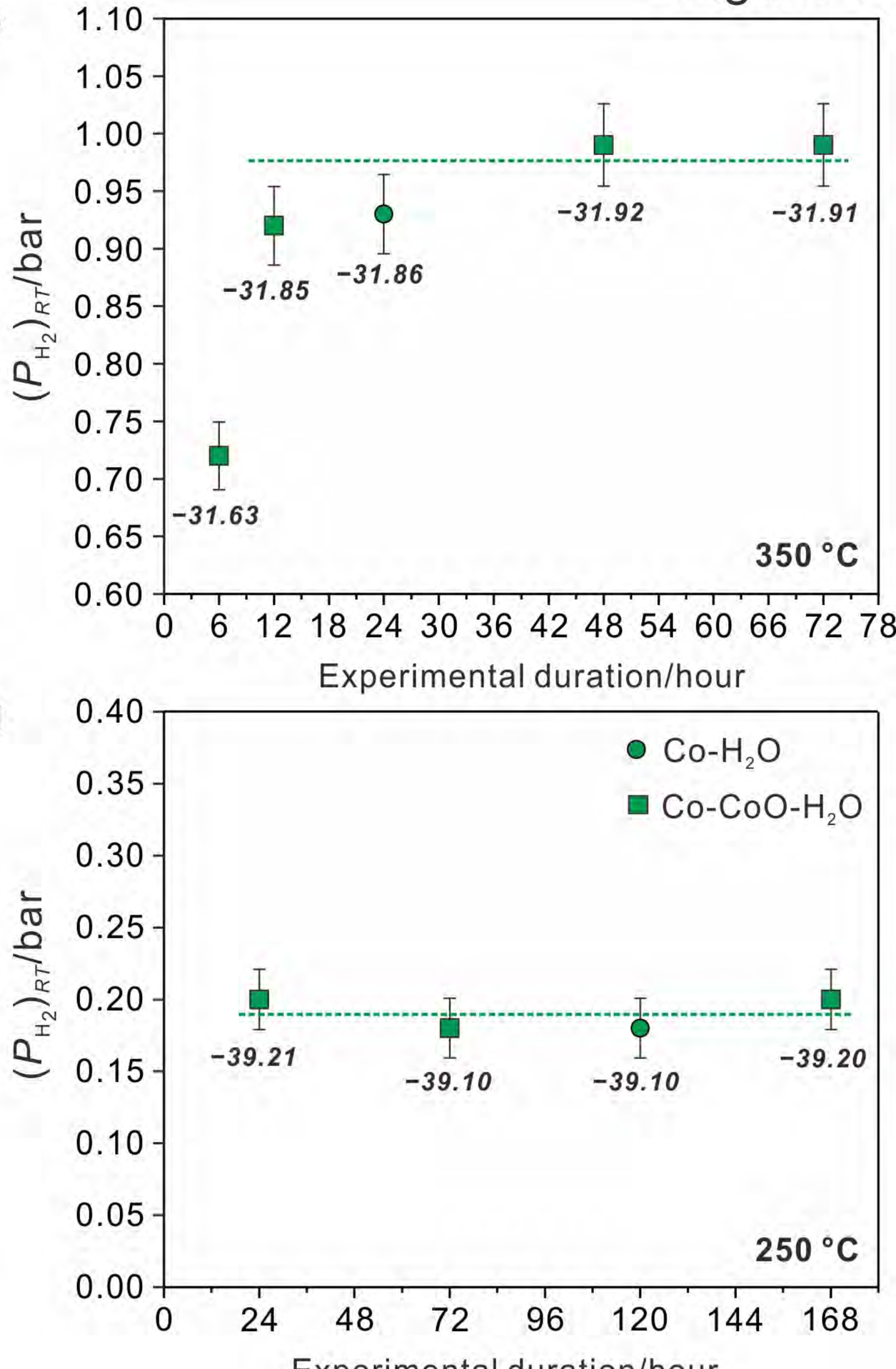
b
$(P_{H_2})_{RT}$/bar
1.10
1.05
1.00
0.95
0.90
0.85
0.80
0.75
0.70
0.65
0.60
−31.63
−31.85
−31.86
−31.92
−31.91
350 °C
0 6 12 18 24 30 36 42 48 54 60 66 72 78
Experimental duration/hour

c
$(P_{H_2})_{RT}$/bar
0.60
0.55
0.50
0.45
0.40
0.35
0.30
0.25
0.20
0.15
0.10
0.05
0.00
−34.11
−35.19
−35.19
−35.26
−35.20
300 °C
0 6 12 18 24 30 36 42 48 54 60 66 72 78
Experimental duration/hour

d
$(P_{H_2})_{RT}$/bar
0.40
0.35
0.30
0.25
0.20
0.15
0.10
0.05
0.00
Co-H_2O
Co-CoO-H_2O
−39.21
−39.10
−39.10
−39.20
250 °C
0 24 48 72 96 120 144 168
Experimental duration/hour

Figure 8

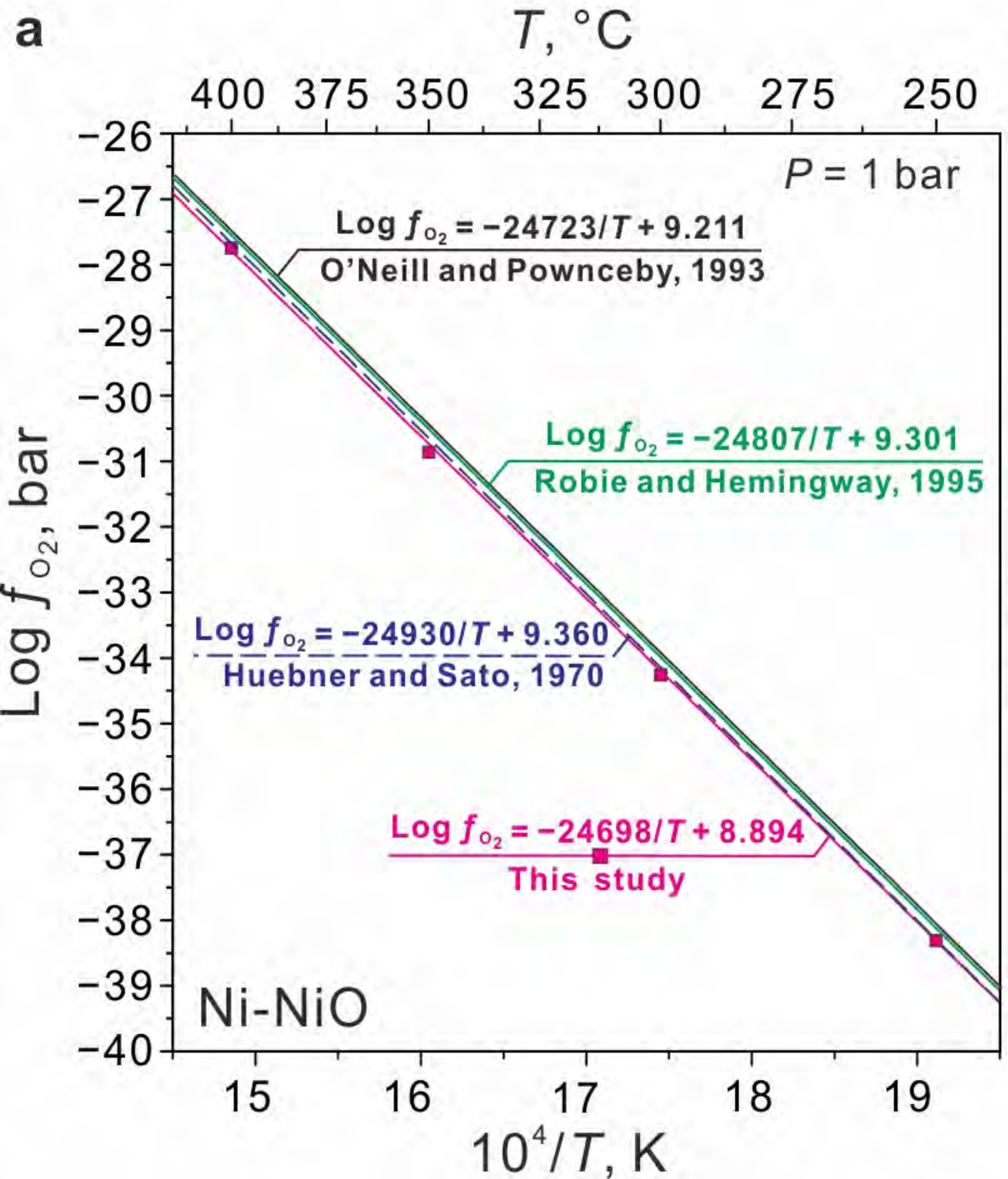
a
T, °C
400 375 350 325 300 275 250
P = 1 bar
Log f_O2 = −24723/T + 9.211
O'Neill and Pownceby, 1993
Log f_O2 = −24807/T + 9.301
Robie and Hemingway, 1995
Log f_O2 = −24930/T + 9.360
Huebner and Sato, 1970
Log f_O2 = −24698/T + 8.894
This study
Ni-NiO
Log f_O2, bar
−26 −27 −28 −29 −30 −31 −32 −33 −34 −35 −36 −37 −38 −39 −40
15 16 17 18 19
10^4/T, K

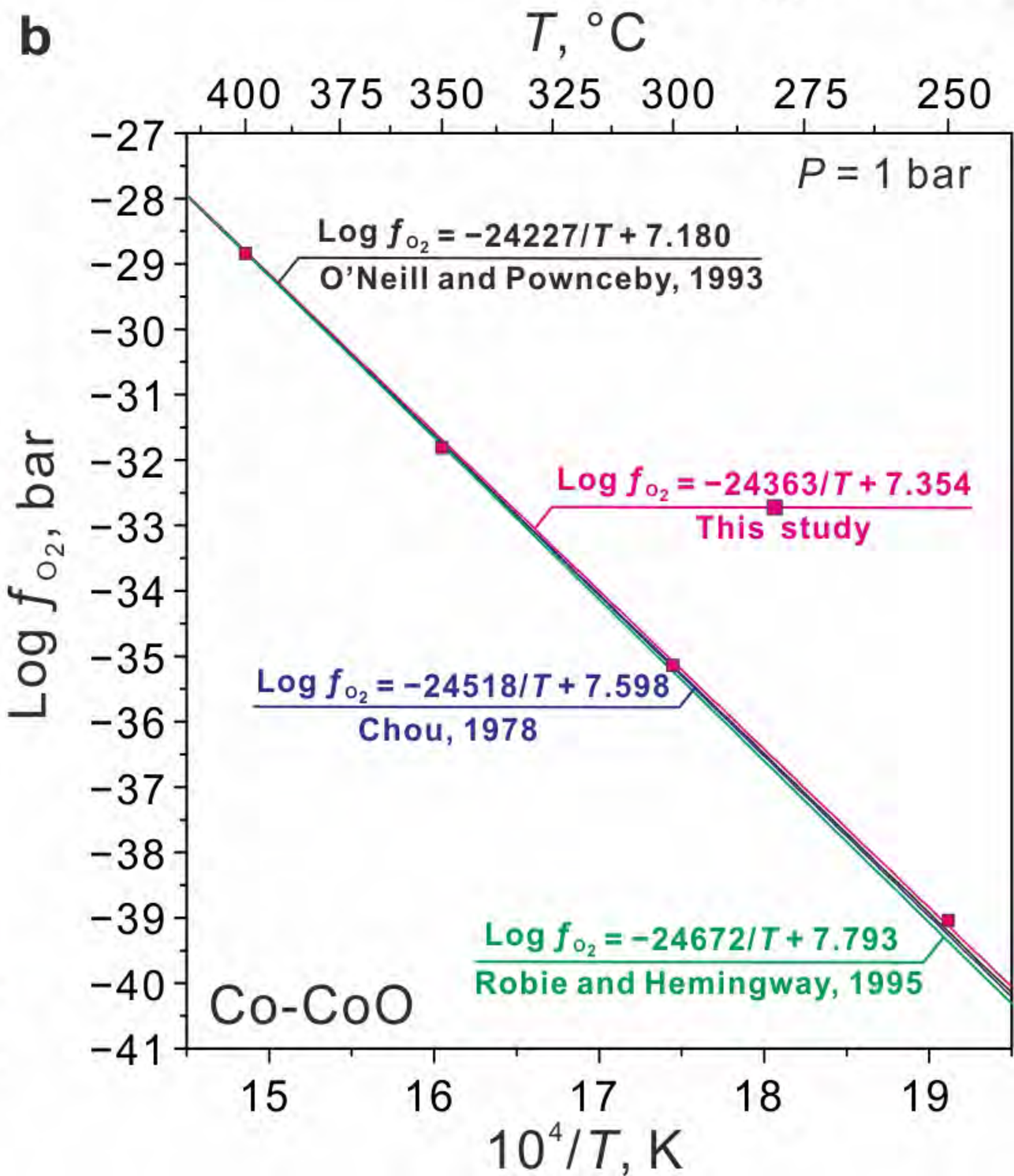
b
T, °C
400 375 350 325 300 275 250
P = 1 bar
Log f_O2 = −24227/T + 7.180
O'Neill and Pownceby, 1993
Log f_O2 = −24363/T + 7.354
This study
Log f_O2 = −24518/T + 7.598
Chou, 1978
Log f_O2 = −24672/T + 7.793
Robie and Hemingway, 1995
Co-CoO
Log f_O2, bar
−27 −28 −29 −30 −31 −32 −33 −34 −35 −36 −37 −38 −39 −40 −41
15 16 17 18 19
10^4/T, K

Table 1. Summary of experimental design

Run type	T (°C)	P (bar)	Duration (hr)	Experimental setup	Imposed H_2/Oxygen buffer	FSCC used	Raman quantitative method
Set-I	350	1	1, 2, 3, 4, 5	Shown in Fig. 1	1 bar H_2	2 CO_2-FSCCs	Raman spectra between 300 and 1500 cm^{-1} were collected from quenched CO_2-FSCCs, and peak height ratios between H_2 and CO_2 were calculated.
	300	1	2, 4, 6, 8, 10, 12	Shown in Fig. 1	1 bar H_2	2 CO_2-FSCCs	
	250	1	4, 8, 12, 16, 20, 24	Shown in Fig. 1	1 bar H_2	2 CO_2-FSCCs	
	200	1	6, 12, 18, 24, 30, 36, 48, 60	Shown in Fig. 1	1 bar H_2	2 CO_2-FSCCs	
	150	1	12, 24, 36, 48, 60, 72, 96, 120	Shown in Fig. 1	1 bar H_2	2 CO_2-FSCCs	
	100	1	48, 72, 96, 120, 168, 192, 216, 264	Shown in Fig. 1	1 bar H_2	2 CO_2-FSCCs	
Set-II	350	Equal to imposed H_2 P	3, 4, 5	Shown in Fig. 1	0.5, 1, 1.5 bar H_2	3 vacuumed FSCCs	Raman spectra of H_2 (4100–4200 cm^{-1}) were collected from quenched vacuumed FSCCs and P of H_2 in them at room T, $(P_{H_2})_{RT}$, and experimental T, $(P_{H_2})_T$, were determined.
	300	Equal to imposed H_2 P	8, 10, 12	Shown in Fig. 1	0.5, 1, 1.5 bar H_2	3 vacuumed FSCCs	
	250	Equal to imposed H_2 P	16, 20, 24	Shown in Fig. 1	0.5, 1, 1.5 bar H_2	3 vacuumed FSCCs	
	200	Equal to imposed H_2 P	36, 48, 60	Shown in Fig. 1	0.5, 1, 1.5 bar H_2	3 vacuumed FSCCs	
Set-III	400	1000	6, 12, 36, 48	Shown in Fig. 2	Ni-NiO	4 vacuumed FSCC	Raman spectra of H_2 (4100–4200 cm^{-1}) were collected from quenched vacuumed FSCCs and $(P_{H_2})_{RT}$ in them were calculated from H_2 peak height; based on $(P_{H_2})_{RT}$, f_{H_2} and f_{O_2} defined by Ni-NiO and Co-CoO buffers at experimental P-T were derived.
	350	1000	6, 12, 36, 48, 96	Shown in Fig. 2	Ni-NiO	4 vacuumed FSCC	
	300	1000	6, 12, 24, 8, 72, 96	Shown in Fig. 2	Ni-NiO	4 vacuumed FSCC	
	250	1000	24, 72, 120, 168	Shown in Fig. 2	Ni-NiO	4 vacuumed FSCC	
	400	1000	6, 12, 24, 36, 48	Shown in Fig. 2	Co-CoO	4 vacuumed FSCC	
	350	1000	6, 12, 24, 48, 72	Shown in Fig. 2	Co-CoO	4 vacuumed FSCC	
	300	1000	6, 12, 24, 8, 72	Shown in Fig. 2	Co-CoO	3 vacuumed FSCC	
	250	1000	24, 72, 120, 168	Shown in Fig. 2	Co-CoO	4 vacuumed FSCC	

Table 2. Comparison of log $(f_{O_2})_{1,T}$ values for Ni-NiO and Co-CoO buffers derived from measured H_2 pressures at room T in present study and those reported previously.

Ni-NiO				
T/°C	[a]log $(f_{O_2})_{1,T}$	[b]log $(f_{O_2})_{1,T}$	[c]log $(f_{O_2})_{1,T}$	[d]log $(f_{O_2})_{1,T}$
400	−27.75 (±0.05)	−27.55	−27.67	−27.52
350	−30.83 (±0.07)	−30.51	−30.65	−30.46
300	−34.15 (±0.13)	−33.98	−34.14	−33.92
250	−38.32 (±0.24)	−38.12	−38.29	−38.05
Co-CoO				
T/°C	[a]log $(f_{O_2})_{1,T}$	[b]log $(f_{O_2})_{1,T}$	[e]log $(f_{O_2})_{1,T}$	[d]log $(f_{O_2})_{1,T}$
400	−28.71 (±0.03)	−28.86	−28.83	−28.81
350	−31.89 (±0.03)	−31.80	−31.74	−31.70
300	−35.21 (±0.05)	−35.25	−35.18	−35.09
250	−39.14 (±0.10)	−39.37	−39.27	−39.13

[a] An average value derived from measured H_2 pressures at room T in quenched vacuumed FSCCs equilibrated with the buffer at 1000 bar and T. All H_2 pressures in vacuumed FSCCs measured at room T are listed in Supplemental Tables S4 and S5, and only those equilibrated values were used. Uncertainty is shown in parentheses and was calculated based on the method described in Appendix C. Note that $(f_{O_2})_{1,T}$ values listed are in bar.

[b] Calculated based on the thermodynamic data of Robie and Hemingway (1995).

[c] Calculated from the log f_{O_2}-T relationship of Huebner and Sato (1970).

[d] Calculated from the μ_{O_2}-T relationship of O'Neill and Pownceby (1993).

[e] Calculated from the log f_{O_2}-T relationship of Chou (1987).